coatings

MDPI

Article

Effect of Different ZrN Addition on Microstructure and Wear Properties of Titanium Based Coatings by Laser Cladding Technique

Xiaodong Li, Shasha Liu, Jiawei Wang, Mengxiao Yu and Haibo Tang *

National Engineering Laboratory of Additive Manufacturing for Large Metallic Components, School of Materials Science and Engineering, Beihang University, Beijing 100191, China; xiaodong.li@buaa.edu.cn (X.L.); shashaliu@buaa.edu.cn (S.L.); jiaweiwang@buaa.edu.cn (J.W.); yumx961219@buaa.edu.cn (M.Y.)

* Correspondence: Tanghb@buaa.edu.cn; Tel.: +86-10-823-39691

Received: 16 March 2019; Accepted: 15 April 2019; Published: 18 April 2019

Abstract: In order to improve the wear resistance of TC11 titanium alloy, a mixture of ZrN (10 wt.%, 20 wt.%, 30 wt.%, and 40 wt.%) and TC11 alloy powders are laser cladded on a forged TC11 substrate. The microstructure and wear property of coatings are systematically analyzed. The results show that the microstructure of sample with 10 wt.% ZrN addition has a very fine α + β two-phase microstructure, powders of ZrN are fully melted with no new phase appearance. By increasing the amount of ZrN to 20 wt.%, new phases of $TiN_{0.3}$ precipitate with the dendritic morphology in the coating. A further increase in ZrN to 30 wt.% and 40 wt.% do not significantly change the microstructure of the cladded layer but increase the microhardness significantly, phases of TiN form with further enhancement of coating hardness. At the bottom of the cladded layer, the morphology of $TiN_{0.3}$ and TiN precipitations changes into a spherical shape with small size. However, the wear performance of the coatings gradually reduces due to the increase of brittleness, and the superior wear properties of the coating are achieved when sample consisted of 20 wt.% ZrN.

Keywords: laser cladding technique; in situ precipitation; titanium; wear property

1. Introduction

TC11 titanium alloy has the advantages of low density, high strength, and excellent corrosion resistance, and it is usually used in the manufacture of large and complex parts such as compressor discs for aircraft engines [1–5]. However, TC11 titanium alloy has low surface hardness with poor wear resistance, which greatly limits its application [6]. Surface modification techniques such as vapor deposition, surface carbonitride, and laser surface treatment are commonly used to improve the wear resistance of titanium alloy [7]. However, traditional carburizing and nitriding may cause the change of microstructures in the alloy, while the bonding strength between the cladding layer and substrate is always very poor when using chemical vapor deposition (CVD) method and physical vapor deposition (PVD) method [8]. The processing times of conventional coating techniques are always long [9]. Laser cladding technology is a newly developed surface modification technology, which can rapidly melt and solidify the pre-mixed powders to obtain a cladding layer with excellent properties. Meanwhile, the bonding strength between the coatings and substrate are excellent, and the coating thickness can be easily adjusted by changing the powdering feeding rates and processing parameters [10–13].

Due to excellent wear properties of ceramic, ceramic phase-enhanced composite coating is always used to improve the wear and corrosion resistance of the titanium alloy. For example, Lin et al. [14] used TiB_2 to enhance the wear property of TC4 titanium alloy by using laser cladding technology. It was found that the bulk and needle-like titanium borides were precipitated in situ from the molten

alloy during solidification. However, due to the fast cooling rate during laser cladding and large hardness differences between reinforced particles and substrate, cracks will easily generate in coatings. For example, Shishkovsky et al. [15] used laser cladding technology to prepare a high hardness Al_2O_3-reinforced Ti-6Al-4Vcoating, but a large number of micro-cracks appeared in coatings with the unsatisfied property.

For titanium alloys, the element of Zr has a similar atomic radius and lattice structure with Ti atoms, which easily form a solid solution. N is an interstitial element that could offer high strengthening effect in titanium. When the contents of N excess its solid solution limit, nitrides are precipitated in alloy, which can further strengthen the matrix [16], because the interface between these in situ phases and alloy matrix is coherent, which will not easily pull out during wear [17]. As it is well-known, ZrN is widely used in the coating of tool steels to improve their wear resistance [18–22]. For example, Floroian et al. [20] and Dias et al. [21] synthesized ZrN wear-resistant coating on the surface of titanium alloy to improve the corrosion resistance of the alloy matrix. In a previous study, Yang et al. [22] indicated that ZrN powders (<12 wt.%) could fully melt and completely dissolve in TC11 alloy, which enhances the microhardness and wear resistance of coating without changing the microstructures of the substrate. In addition, the oxidation resistance of nitride is excellent [23], and the solid-solution N in the alloy matrix can also increase the oxidation properties of the coating [24]. In this study, high amount of ZrN powders (10 wt.%, 20 wt.%, 30 wt.%, and 40 wt.%), are added into TC11 alloy to further enhance its wear property by in situ forming titanium nitride. Then, the microstructure of the coating, coating/substrate interface, and heat affected zone were analyzed. Moreover, the hardness and wear resistance of the coating were characterized.

2. Materials and Methods

The substrate selected in this paper is a forged TC11 titanium alloy plate with a size of 100 mm × 75 mm × 40 mm. ZrN powder was mixed with TC11 powder (shown in Figure 1) in a ratio of 10 wt.% (10ZrN), 20 wt.% (20ZrN), 30 wt.% (30ZrN), and 40 wt.% (40ZrN). The mixed powders were mixed on a ball mill (QM-2SP12-CL) at a rotation speed of 200 rev/min for 1 h. After that, powders were evenly coated on the TC11 substrate, and then a high-energy CO_2 laser beam was applied on the surface of mixed powders. Based on a previous study [22], the optimized processing parameters were used in this study with a power of 6 kW, a spot diameter of 5 mm, and a scanning speed of 600 nm/min. During the entire laser cladding process, an inert gas is applied for protecting the oxidation of alloy. Finally, a uniform crack-free cladding layer having a thickness of 2 mm is coated on the surface of TC11 alloy.

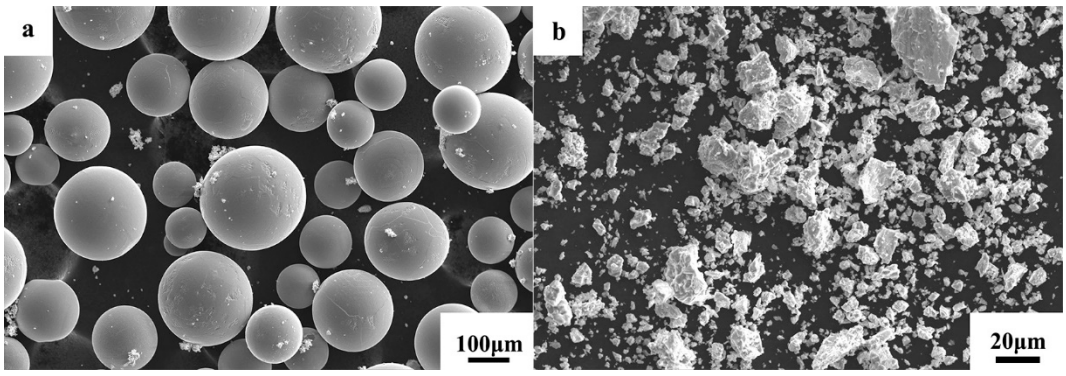

Figure 1. SEM micrographs of (**a**) TC11 powders and (**b**) ZrN powders.

The microstructure of coatings was characterized using an optical microscope (OM, LEICA DM4000, Wetzlall, Germany), scanning electron microscope (SEM, JSM6010, JEOL, Tokyo, Japan), and a JEOL, JXA-8100 electron probe micro-analyzer (EPMA). Phases in samples were characterized using a Rigaku D/MAX-2500 X-ray diffractometer (Tokyo, Japan). The microstructure of the coating was observed using backscattered electron images, and the composition of coating was analyzed by

EPMA. The microhardness of the samples was measured by a Constant-FM800 microhardness tester (Tokyo, Japan) with a test load of 500 g, a loading time of 10 s, and an average of three measurements were used for the microhardness tests. In order to characterize the hardness of the TiN and the matrix, nano-indentation test (Bruker UMT-2 nanoindentor, Billerica, MA, USA) was performed with a maximum load of 50 mN and dwell time of 10 s. Meanwhile, the Pin-on-disc dry sliding wear tests were conducted on a Plint TE-92 wear tester (Phoenix Tribology Ltd, Berkshire, UK) to analyze wear resistance of coatings. The GCr15 bearing steel was selected as the grinding pair. The test parameters were listed: Sample size $\Phi = 7.8 \times 20$ mm^2, load 30 N, testing time of 60 min, the line speed is 0.5 m/s, the rotation speed is 200 rpm, the wear test distance is 1800 m, and an average of three measurements were used for the wear tests. The wear resistance of the material is characterized by mass loss and the change of morphology of worn surfaces.

3. Results

3.1. Microstructures and Compositions

The microstructure of coatings with different ZrN additions is shown in Figure 2. When the addition amount of ZrN is 10 wt.%, coating shows a uniform α + β basket-weave microstructure without the observation of new phase, which is consistent with the results of Yang et al. [22]. When the addition amount of ZrN increases to 20 wt.%, precipitations with dendritic morphology start to precipitate from the matrix with α + β basket-weave microstructure. Moreover, the number of dendritic precipitations increase with an increase in the amount of ZrN. The backscattered electron analysis results shown in Figure 3 indicate that the shape of precipitates changes from the dendritic morphology to spherical shape at the bottom of the coating.

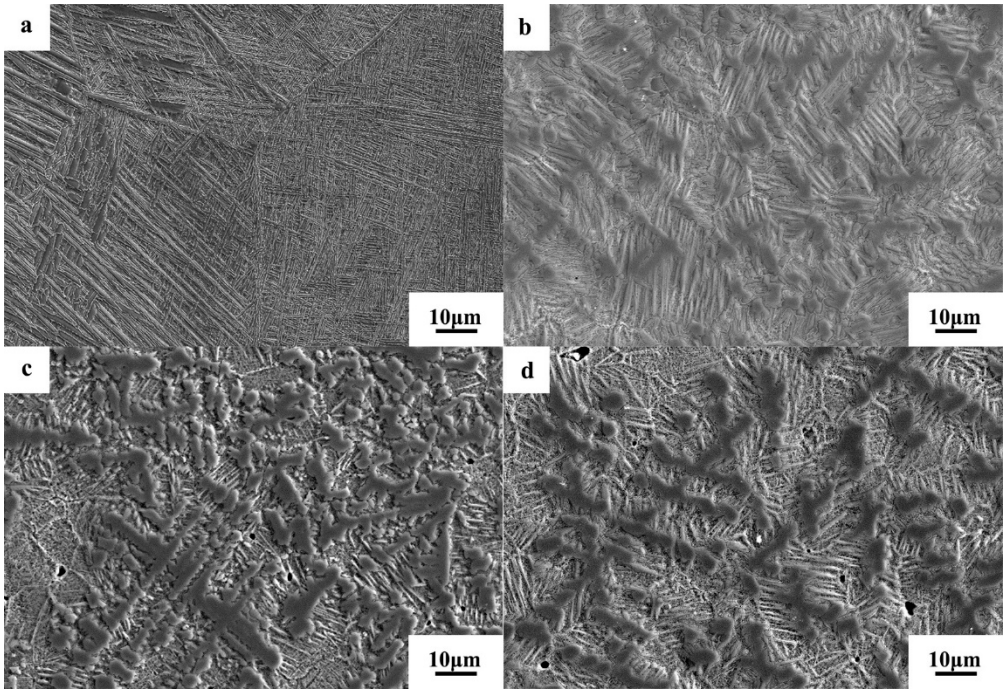

Figure 2. Microstructures of the coating with different ZrN additions (**a**) 10 wt.% (10ZrN), (**b**) 20 wt.% (20ZrN), (**c**) 30 wt.% (30ZrN), and (**d**) 40 wt.% (40ZrN).

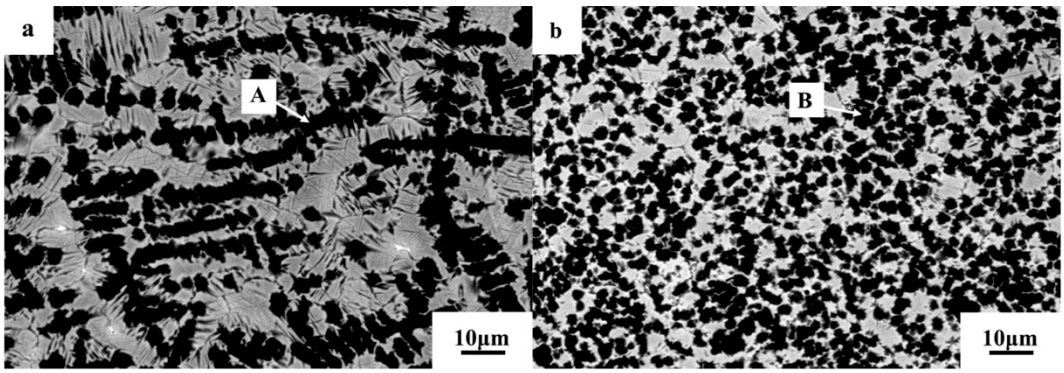

Figure 3. Backscattered electron micrograph of the coating of 30ZrN at different locations; (**a**) at the top of the coating and (**b**) at the bottom of the coating.

EPMA analysis results of the compositions of the alloy at different locations in Figure 3 are listed in Table 1. As it can be seen that the substrate contains high amount of solid-solution Zr (11.61 wt.%, N is a light element which could not be measured accurately by EPMA). At the top of the layer, the phase with dendritic morphology contains around 22 wt.% Zr (position A), and spherical phase in the bottom has the highest Zr contents of around 30 wt.% (position B).

Table 1. Electron probe micro-analyzer (EPMA) analysis of different position components of the coating of 30ZrN.

Position	Zr wt.%	Ti wt.%	Al wt.%
A	22.10	77.54	0.36
B	30.65	68.64	0.71
TC11Titaniumalloy matrix	11.61	82.32	6.07

XRD results of coatings are different, see Figure 4. It can be seen that when there is an addition of 10 wt.% ZrN in the coating, there is no new phase form, and the main phases are an α-Ti phase and β-Ti phase. Moreover the solid-solution of Zr and N in the coating does not cause the broadening of peaks but leads to the shifting of α-Ti phase and β-Ti phase towards low angle region about 2°. When increasing the ZrN addition to 20 wt.%, a new phase of $TiN_{0.3}$ was formed (non-stoichiometric TiN compound, N-deficient solid solution). For samples containing 30 wt.% and 40 wt.% ZrN, besides of $TiN_{0.3}$ phase, precipitation of TiN appears. According to the research carried out by Yu et al. [25], Ti and N can form TiN_x compounds with varying N contents: x = 0.3 to 1. Sridar et al. [26] state that the element of Ti, Zr, and N can completely miscible at 2000 K, the possible phases in the Ti-Zr-N system is (Ti,Zr) (N,Va), where Va states the vacancy. In this study, high Zr concentration is detected in the titanium nitrides, according to the EPMA results. Hence, the new phases appearing in this study should be $(Ti,Zr)N_{0.3}$ and (Ti,Zr)N.

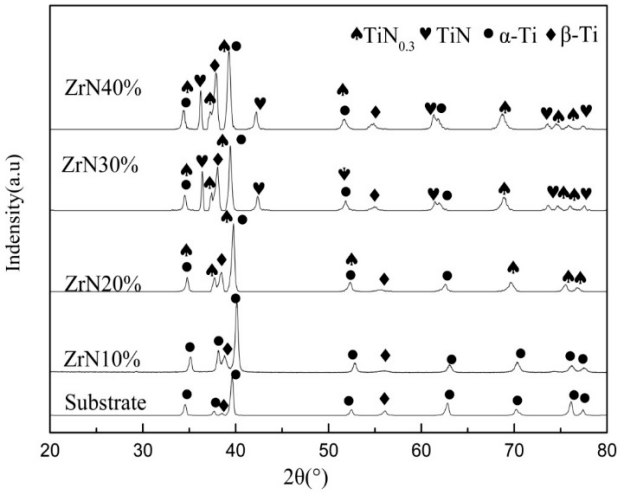

Figure 4. XRD spectra of the coatings and substrate.

Figure 5 shows the microstructure changes of 30ZrN sample from the coating to the substrate. The overall microstructure can be divided into three parts as coating, heat affected zone (HAZ), and matrix. As mentioned above, dendritic precipitations only appear on the top of the coating, and at the bottom of the coating, the morphology of precipitates changes into a spherical shape. The average Zr concentration for sample 30ZrN from the coating to the substrate is listed in Figure 6. As it is shown, the average Zr concentration in the coating is around 25 wt.%, and then it gradually decreases towards the metal substrate by forming a transition zone with a thickness of around 200 μm at the coating-substrate interface. The HAZ consists of equiaxed grains with α + β basket-weave microstructure.

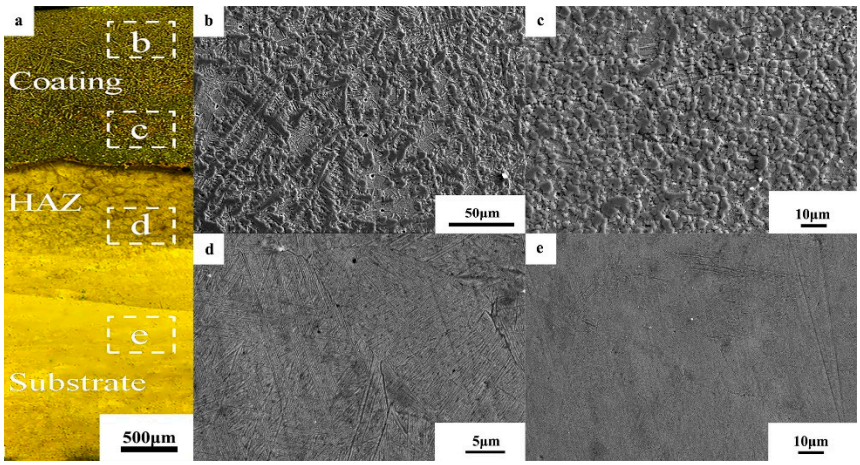

Figure 5. (**a**) Optical microscope (OM) microstructures of the cross-section of sample 30ZrN, SEM image of (**b**) the top of the coating, (**c**) the bottom of the coating, (**d**) heat affected zone (HAZ), and (**e**) forged titanium alloy substrate.

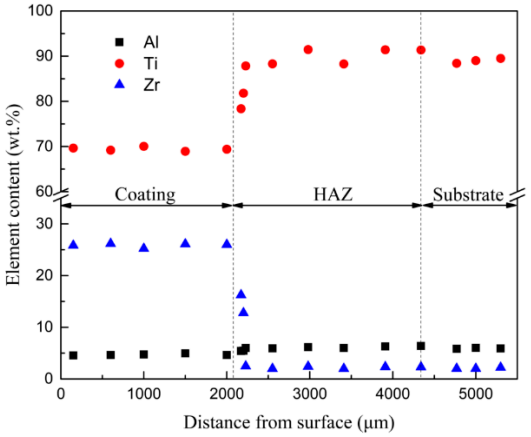

Figure 6. Elemental distribution at different distance away from surface (30ZrN).

3.2. *Microhardness and Wear Resistance*

Microhardness of the coatings with different ZrN additions is illustrated in Figure 7. All the coatings have high hardness, and by increasing the ZrN concentration, the hardness increases from 350 Hv for TC11 substrate to 800 Hv for coating with 40 wt.% ZrN addition. When the addition of ZrN exceeds 30 wt.%, a further change of ZrN concentration does not cause a continuous increase of hardness in the coatings. Increasing the distance from the coating, the microhardness gradually drops. Attributed to the element diffusion, the sample of 40ZrN has the widest transition zone thickness (~1000 μm). In addition, nano-indentation results indicated in Figure 8 show that the titanium nitride has a very high hardness of 9.7 Gpa, and due to the strong solid-solution effects of Zr and N elements, the metal matrix also has a high hardness of 7.38 Gpa.

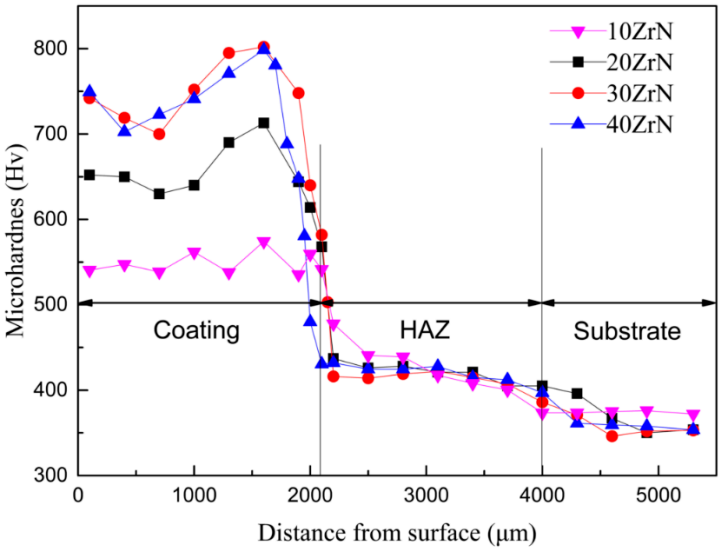

Figure 7. Microhardness of samples with different ZrN additions.

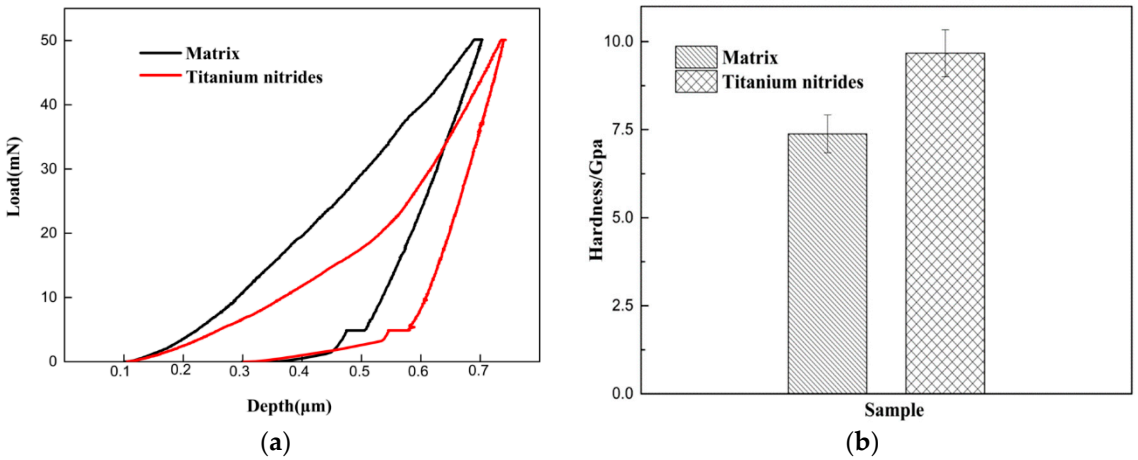

Figure 8. (**a**) Nano-indentation load-depth curves for precipitations (TiN) and matrix of 30ZrN, and (**b**) hardness of precipitations (TiN) and matrix of 30ZrN.

After the wear test, the mass loss of the different coatings is illustrated in Figure 9. It can be seen that the mass loss of the substrate is 96(±2.7) mg, after addition of 10 wt.% of ZrN, the weight loss dramatically decreases to 54(±1.90) mg. With further increase in the ZrN to 20 wt.%, the weight loss continued to decrease to 50(±2.50) mg. However, when the addition amount of ZrN exceeds 30 wt.%, the weight loss of the coating increases again with similar weight loss observed in the sample of 40ZrN and substrates. Sample 20ZrN shows the best wear resistance and mass loss, which is only one-half of the titanium alloy matrix.

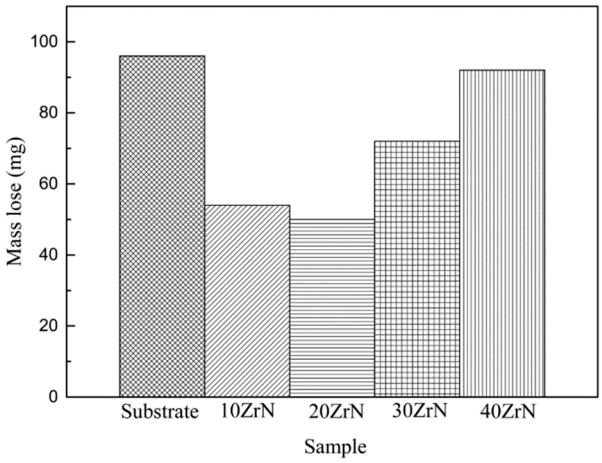

Figure 9. Mass loss of different coatings after pin-on-disc dry sliding wear test.

The wear surface of the coating and the morphology of wearing debris are indicated in Figure 10. It can be seen that after the wearing test, the surface of TC11 alloy without coatings has very rough microstructures with many debris. After addition of ZrN for 10 wt.%, the surface of the coating becomes smoother, only some scratches are observed on the surface with decreased of size of the debris. The 20ZrN sample has the smoothest surface with the smallest debris. Similar to the weight loss, the further addition of ZrN to 30 wt.% and 40 wt.% cause the increasing roughness of the coating after the wear test. Sample of 40ZrN has similar surface morphology as the original TC11 substrate.

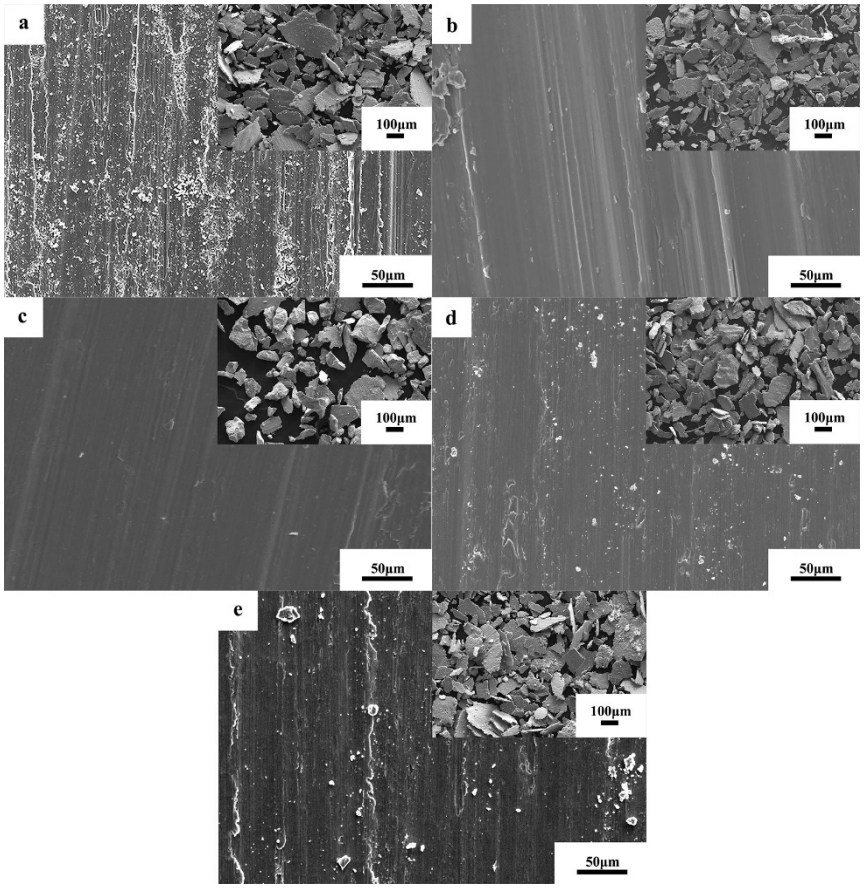

Figure 10. Surface morphology of coatings after dry-sliding wear test (**a**) substrate, (**b**) 10ZrN, (**c**) 20ZrN, (**d**) 30ZrN, and (**e**) 40ZrN.

4. Discussion

4.1. Microstructure Evolution at Different ZrN Additions

In this study, different amounts of ZrN are mixed with TC11 powders to form coatings with in situ formations of titanium nitride precipitations to improve the wear resistance of the titanium alloy. Titanium nitride is also reported to have other benefits to improve the oxidation resistance of titanium alloys [27], and coatings are supposed to have good oxidation properties.

When the additional amount of ZrN less than 10 wt.%, both Zr and N elements can completely solid solution in TC11 alloy. When the ZrN addition amount exceeds 20 wt.%, phases of $(Ti,Zr)N_{0.3}$ precipitate out from alloy matrix with dendritic microstructure. Further increase of ZrN contents to 30 wt.% and 40 wt.% will increase the number of titanium nitride phases, and the volume fraction of $(Ti,Zr)N_x$ could reach to around 60% in the coating when 40 wt.% ZrN is added.

However, microstructures of the coatings at cross-sections indicate that the morphology of titanium nitride changes from the dendritic structure to spherical structure at the location close to the bottom of the coating (close to the coating/heat affected zone boundary). In addition, the observation in Figure 11 indicates that the precipitations in the bottom are small with high density. As the distance increase away from the bottom, the size of precipitation increases, and some of them already have a dendritic shape with under-developed arms. Since there is no evidence is found about the existence of original ZrN particles (un-melt) in the coatings. The change of morphology of precipitations may occur due to the change of solidification times, or due to the Marangoni flows in the molten pool during solidification [28]. As it was known, the bottom of the coating is the first place to solidify with very fast cooling rate (~10^5 K/s) [29], and the temperature gradient (G) in this region is also very high,

resulting of a comparably low G/V ratio, where the V states solidification velocity. The morphology of precipitations is dependent on the G/V ratios. For example, planner growth is enhanced for the large G/V ratio, and for low G/V ratio, equiaxed dendritic growth of precipitations is preferred [30]. Hence the (Ti,Zr)N_x precipitates with equiaxed morphology only appear at the areas close to the bottom of the molten pool. Besides, the solidification condition of molten pool is very complicated, and the fluid turbulence [27] may cause the dendrite to break or disturb the growth of dendrite, leading to the formation of equiaxed (Ti,Zr)N_x precipitates.

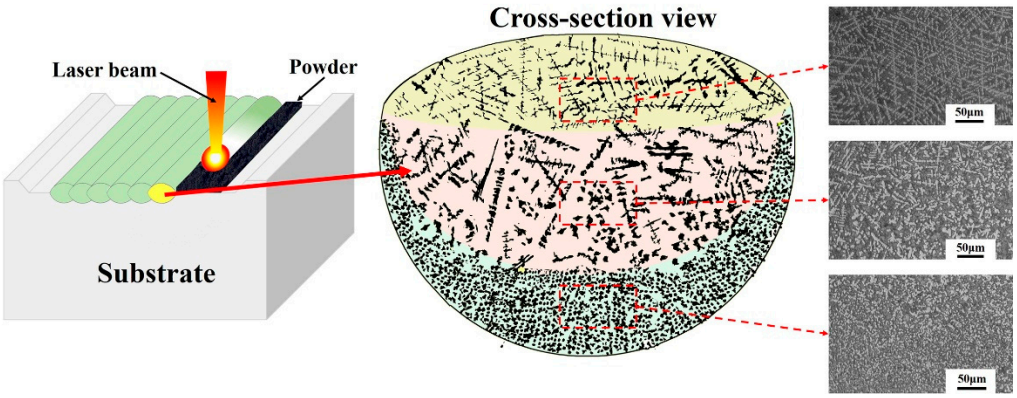

Figure 11. Change morphology of precipitations in coatings (30ZrN).

4.2. Effect of Different ZrN Addition on the Friction and Wear Properties of Coatings

The microhardness of the coatings with different ZrN additions is shown in Figure 7. All the laser cladded samples exhibited high microhardness. With the increase of ZrN addition, the microhardness of the coating increases from 530 Hv (10ZrN) to 800 Hv (40ZrN). The increasing hardness of the coatings may both come from the precipitation strengthening effect of new precipitated (Ti,Zr)$N_{0.3}$ and (Ti,Zr)N phase, see Figure 8 (nano-indentation test), and from solid solution strengthening of Zr and N elements (the alloy matrix has high hardness of 7.38 Gpa). However, there is an obvious increase of microhardness observed at the bottom of the coating in sample 20ZrN, 30ZrN, and 40ZrN, which contained the titanium nitride strengthening phases. By careful calculation of the fraction of precipitation phases, the top of the layer contains of 56 vol.% of titanium nitride, and for the bottom of the layer, it contains higher amount of titanium nitride of 62%. Therefore, the high hardness of the coating at the coating/substrate interface may attribute to finer (Ti,Zr)N_x precipitations with higher density. In addition, the residual stress in coatings may also cause an increase of hardness in the coatings [31,32]. However, comparing with the larger strengthening effect from precipitations and solid-solution elements, the attribution of the results stress that the hardness can be ignored.

Although microhardness of the coatings increases with increasing ZrN contents, wear resistance of the coating increases firstly and then shows a decreasing tendency. The coating has the best wear resistance when the amount of ZrN is 20 wt.%. When the addition amount exceeds 30 wt.%, coatings become very brittle (both due to the high solidification of Zr and N element and the large quantity of (Ti, Zr)N_x precipitates). During wearing test, coating easily delaminated, which may attribute both the solid-solution effect from elements (especially N) and the weak bonding between precipitation and TC11 matrix.

5. Conclusions

In this paper, ZrN reinforced titanium-based composite coating was prepared on the surface of titanium alloy by laser cladding technology. This paper focuses on the change of microstructures and wear resistances of samples. The conclusion is as follows:

- New precipitation such as $TiN_{0.3}$ and TiN are in situ precipitated in the coating when the addition of ZrN exceeds 20 wt.%. TiN_x based precipitates have dendritic morphology at the top of the coating, and which change to a spherical shape at the bottom of the molten pool.
- As the ZrN contents increase, the hardness of the coating increases significantly. The increase in microhardness of the coating is mainly due to the in situ formation of TiN_x reinforcing phase and solid solution strengthening of elements such as Zr and N.
- The enhanced microhardness of the coatings could improve the wear properties, and high amount of ZrN addition (20 wt.% ZrN) will lead to embrittlement of the coatings; then, their wear resistance degrades.

Author Contributions: Conceptualization, X.L. and H.T.; Methodology, J.W.; Software, S.L. and J.W.; Validation, J.W.; Formal Analysis, X.L.; Investigation, S.L. and M.Y.; Resources, M.Y.; Data Curation, S.L. and J.W.; Writing—Original Draft Preparation, X.L.; Writing—Review and Editing, H.T.; Visualization, S.L.; Supervision, J.W.; Project Administration, H.T.; Funding Acquisition, H.T.

Funding: This research was funded by National Key Research and Development Program (No. 2018YFB1105804, No. 2016YFB1100400) and Beijing Municipal Science and Technology Project (No. Z181100003318001).

Conflicts of Interest: The authors declare no conflicts of interest.

References

1. Christoph, L.; Manfred, P. *Titanium and Titanium Alloys: Fundamentals and Applications*; Wiley-VCH: Köln, Germany, 2003.
2. Peters, M.; Kumpfert, J.; Ward, C.H.; Leyens, C. Titanium alloys for aerospace applications. *Adv. Eng. Mater.* **2003**, *5*, 419–427. [CrossRef]
3. Lütjering, G.; Williams, J.C. *Titanium*, 2nd ed.; Springer: Berlin, Germany, 2007.
4. Bruni, S.; Martinesi, M.; Stio, M.; Treves, C.; Bacci, T.; Borgioli, F. Effects of surface treatment of Ti–6Al–4V titanium alloy on biocompatibility in cultured human umbilical vein endothelial cells. *Acta Biomater.* **2005**, *1*, 223–234. [CrossRef] [PubMed]
5. Boyer, R.R. An overview on the use of titanium in the aerospace industry. *Mater. Sci. Eng. A* **1996**, *213*, 103–114. [CrossRef]
6. Zhang, L.; Lu, J.Z.; Zhang, Y.K.; Luo, K.Y.; Zhong, J.W.; Cui, C.Y.; Kong, D.J.; Guan, H.B.; Qian, X.M. Effects of different shocked paths on fatigue property of 7050-T7451 aluminum alloy during two-sided laser shock processing. *Mater. Des.* **2011**, *32*, 480–486. [CrossRef]
7. Saleh, A.F.; Abboud, J.H.; Benyounis, K.Y. Surface carburizing of Ti–6Al–4V alloy by laser melting. *Opt. Lasers Eng.* **2010**, *48*, 257–267. [CrossRef]
8. Weng, F.; Chen, C.; Yu, H. Research status of laser cladding on titanium and its alloys: A review. *Mater. Des.* **2014**, *58*, 412–425. [CrossRef]
9. Höche, D.; Kaspar, J.; Schaaf, P. Laser nitriding and carburization of materials. In *Laser Surface Engineering*; Woodhead Publishing: Sawston, Cambridge, UK, 2014; pp. 33–58.
10. Liu, J.; Li, L. Study on cross-section clad profile in coaxial single-pass cladding with a low-power laser. *Opt. Laser Technol.* **2005**, *37*, 478–482. [CrossRef]
11. Wu, P.; Du, H.M.; Chen, X.L.; Li, Z.Q.; Bai, H.L.; Jiang, E.Y. Influence of WC particle behavior on the wear resistance properties of Ni–WC composite coatings. *Wear* **2004**, *257*, 142–147. [CrossRef]
12. Savalani, M.M.; Ng, C.C.; Li, Q.H.; Man, H.C. In situ formation of titanium carbide using titanium and carbon-nanotube powders by laser cladding. *Appl. Surf. Sci.* **2012**, *258*, 3173–3177. [CrossRef]
13. Lifang, C.; Zhang, Y.; Likai, S. Microstructure and formation mechanism of titanium matrix composites coating on Ti-6Al-4V by laser cladding. *Rare Met.* **2007**, *26*, 342–346.
14. Lin, Y.; Chen, Z.; Li, Y.; Zhu, W.; Wen, X.; Wang, X. Microstructure and hardness characteristic of in-situ synthesized TiB coating by laser cladding on TC4 titanium alloy. *Infrared Laser Eng.* **2012**, *41*, 2694–2698. (In Chinese)
15. Shishkovsky, I.; Smurov, I. Titanium base functional graded coating via 3D laser cladding. *Mater. Lett.* **2012**, *73*, 32–35. [CrossRef]

16. Tavares, C.J.; Rebouta, L.; Almeida, B.; Sousa, J.B.E. Structural characterization of multilayered sputtered TiN/ZrN coatings. *Surf. Coat. Technol.* **1998**, *100–101*, 65–71. [CrossRef]
17. Lin, Y.C.; Lin, Y.C.; Chen, Y.C. Evolution of the microstructure and tribological performance of Ti–6Al–4V cladding with TiN powder. *Mater. Des. (1980–2015)* **2012**, *36*, 584–589. [CrossRef]
18. Deng, J.; Liu, J.; Zhao, J.; Song, W. Wear mechanisms of PVD ZrN coated tools in machining. *Int. J. Refract. Met. Hard Mater.* **2008**, *26*, 164–172. [CrossRef]
19. Bobzin, K. High-performance coatings for cutting tools. *CIRP J. Manuf. Sci. Technol.* **2017**, *18*, 1–9. [CrossRef]
20. Floroian, L.; Craciun, D.; Socol, G.; Dorcioman, G.; Socol, M.; Badea, M.; Craciun, V. Titanium implants' surface functionalization by pulsed laser deposition of TiN, ZrC and ZrN hard films. *Appl. Surf. Sci.* **2017**, *417*, 175–182. [CrossRef]
21. Dias, F.C.; Silva, C.R.; Muterlle, P.V.; Henriques, V.A.; Araújo, J.A. Wear resistance of Ti-40Zr alloy with TiN and ZrN multilayer coatings. *Adv. Mater. Res.* **2014**, *936*, 1056–1065. [CrossRef]
22. Yang, C.; Cheng, X.; Tang, H.; Tian, X.; Liu, D. Influence of microstructures and wear behaviors of the microalloyed coatings on TC11 alloy surface using laser cladding technique. *Surf. Coat. Technol.* **2018**, *337*, 97–103. [CrossRef]
23. Liu, H.; Zhang, X.; Jiang, Y.; Zhou, R. Microstructure and high temperature oxidation resistance of in-situ synthesized TiN/Ti3Al intermetallic composite coatings on Ti6Al4V alloy by laser cladding process. *J. Alloy. Compd.* **2016**, *670*, 268–274. [CrossRef]
24. Nie, G.Z.; Zhong, C.L.; Luo, L.E.; Zhou, R.L.; Liu, Q. Microstructure and oxidation resistance of TiN coatings. *Adv. Mater. Res.* **2013**, *750–752*, 2092–2095. [CrossRef]
25. Yu, S.; Zeng, Q.; Oganov, A.R.; Frapper, G.; Zhang, L. Phase stability, chemical bonding and mechanical properties of titanium nitrides: A first-principles study. *Phys. Chem. Chem. Phys.* **2015**, *17*, 11763–11769. [CrossRef]
26. Sridar, S.; Kumar, R.; Kumar, K.C.H. Thermodynamic modelling of Ti-Zr-N system. *Calphad* **2017**, *56*, 102–107. [CrossRef]
27. Gurrappa, I.; Manova, D.; Gerlach, J.W.; Mändl, S.; Rauschenbach, B. Influence of nitrogen implantation on the high temperature oxidation of titanium-base alloys. *Surf. Coat. Technol.* **2006**, *201*, 3536–3546. [CrossRef]
28. Bai, X.; Colegrove, P.; Ding, J.; Zhou, X.; Diao, C.; Bridgeman, P.; Roman Hönnige, J.; Zhang, H.; Williams, S. Numerical analysis of heat transfer and fluid flow in multilayer deposition of PAW-based wire and arc additive manufacturing. *Int. J. Heat Mass Transfer* **2018**, *124*, 504–516. [CrossRef]
29. Wang, Z.J.; Luo, S.; Song, H.W.; Deng, W.D.; Li, W.Y. Simulation of microstructure during laser rapid forming solidification based on cellular automaton. *Math. Prob. Eng.* **2014**, *2014*, 627528. [CrossRef]
30. David, S.A.; Vitek, J.M. Correlation between solidification parameters and weld microstructures. *Int. Mater. Rev.* **1989**, *34*, 213–245. [CrossRef]
31. Ghidelli, M.; Sebastiani, M.; Collet, C.; Guillemet, R. Determination of the elastic moduli and residual stresses of freestanding Au-TiW bilayer thin films by nanoindentation. *Mater. Des.* **2016**, *106*, 436–445. [CrossRef]
32. Suresh, S.; Giannakopoulos, A.E. A new method for estimating residual stresses by instrumented sharp indentation. *Acta Mater.* **1998**, *46*, 5755–5767. [CrossRef]